Inorg. Chem. **2007**, *46*, 8668–8675

Structurally Homologous β- and *meso*-Alkynyl Amidinium Porphyrins

Joel Rosenthal, Elizabeth R. Young, and Daniel G. Nocera*

Department of Chemistry, 6-335, Massachusetts Institute of Technology, 77 Massachusetts Avenue, Cambridge, Massachusetts 02139-4307

Received May 1, 2007

Alkynylamidinium groups have been introduced at the β and *meso* positions of a nickel(II) porphyrin (PNi(II)) framework. The modification permits the distance between the amidinium–amidine acid–base group and porphyrin to be increased while effectively maintaining π conjugation between the porphyrin macrocycle and the acid–base functionality. Use of an ethynyl spacer as a linker (i) extends the amidinium functionality away from the sterically bulky mesityl groups of the porphyrin, allowing it to be nearly planar with respect to the porphyrin ring, and (ii) draws the π-orbital character of the porphyrin out toward the amidinium functionality, thereby engendering sensitivity of the electronic properties of the porphyrin macrocycle to the protonation state of the amidinium. The barrier for rotation of the amidinium group, as calculated by time-dependent density functional theory (TDDFT), is $\sim$8.5kT (5 kcal/mol) for both porphyrins. Analysis of UV–visible absorption profiles for the β- and *meso*-alkynylamidinium PNi(II) upon deprotonation enables accurate determination of the amidinium acidity constants for the ground state (pK_a(β) = 7.03 ± 0.1, pK_a(*meso*) = 7.74 ± 0.1 in CH_3CN) and excited state (pK_a*(β) = 6.89 ± 0.1, pK_a*(*meso*) = 8.37 ± 0.1 in CH_3CN) porphyrins. Whereas pK_a* < pK_a for the β-alkynylamidinium porphyrin, pK_a* > pK_a for the *meso*-alkynylamidinium porphyrin, indicating that β-alkynylamidinium PNi(II) is a photoacid and *meso*-alkynylamidinium PNi(II) is a photobase. These divergent behaviors are supported by analysis of the frontier molecular orbitals of the homologous pair with TDDFT.

Introduction

Supramolecular porphyrin assemblies constructed from donor (D) and acceptor (A) termini bridged by a hydrogen-bond network ([H^+]) may be used for the study of photoinduced proton-coupled electron transfer (PCET).[1] Initial D−[H^+]−A assemblies employed dicarboxylic acid dimers[2,3] and Watson−Crick base pairs as [H^+].[4] Subsequent studies showed that the [H^+] interface exerts its greatest influence on the PCET event when it is asymmetric and capable of supporting proton transfer.[5−7] For these reasons, we have focused on photoinduced charge transport mediated by amidinium-carboxylate interfaces.[8] The amidinium-carboxylate salt-bridge combines the dipole of an electrostatic ion pair interaction within a hydrogen-bonding scaffold and allows for the investigation of the manner in which proton motion within a hydrogen-bond interface affects the charge, energetics, and electronic coupling of electron transport.[1,7−10] The charge shift resulting from the motion of the proton can couple to the charge shift of the electron transfer through the polarization of the surrounding environment.[11−15] It is this mechanism that distinguishes electron-transfer (ET) from PCET.

The kinetics for the individual proton-transfer (PT) and ET steps of the photoinduced PCET event may be probed by transient spectroscopy as long as the PT and ET are

* To whom correspondence should be addressed. E-mail: nocera@mit.edu.

(1) Chang, C. J.; Brown, J. D. K.; Chang, M. C. Y.; Baker, E. A.; Nocera, D. G. In *Electron Transfer in Chemistry*; Balzani, V., Ed.; Wiley-VCH: Weinheim, Germany, 2001; Vol. 3.2.4, pp 409−461.
(2) Turró, C.; Chang, C. K.; Leroi, G. E.; Cukier, R. I.; Nocera, D. G. *J. Am. Chem. Soc.* **1992**, *114*, 4013−4015.
(3) de Rege, P. J. F.; Williams, S. A.; Therien, M. J. *Science* **1995**, *269*, 1409−1413.
(4) Sessler, J. L.; Wang, B.; Springs, S. L.; Brown, C. T. In *Comprehensive Supramolecular Chemistry*; Murakami, Y., Ed.; Pergamon Press: Oxford, 1996; Vol. 4, pp 311−336 and references therein.
(5) Roberts, J. A.; Kirby, J. P.; Nocera, D. G. *J. Am. Chem. Soc.* **1995**, *117*, 8051−8052.
(6) Roberts, J. A.; Kirby, J. P.; Wall, S. T.; Nocera, D. G. *Inorg. Chim. Acta* **1997**, *263*, 395−405.
(7) Kirby, J. P.; Roberts, J. A.; Nocera, D. G. *J. Am. Chem. Soc.* **1997**, *119*, 9230−9236.
(8) Damrauer, N. H.; Hodgkiss, J. M.; Rosenthal, J.; Nocera, D. G. *J. Phys. Chem. B* **2004**, *108*, 6315−6321.
(9) Chang, C. J.; Chang, M. C. Y.; Damrauer, N. H.; Nocera, D. G. *Biophys. Biochim. Acta* **2004**, *1655*, 13−28.
(10) Hodgkiss, J. M.; Damrauer, N. H.; Pressé, S.; Rosenthal. J.; Nocera, D. G. *J. Phys. Chem. A* **2006**, *110*, 18853−18858.

10.1021/ic700838s CCC: $37.00
Published on Web 09/14/2007

Scheme 1

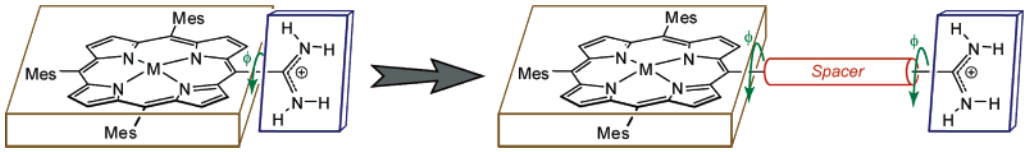

spectroscopically distinguished. This task is not particularly onerous for ET but does present challenges for PT. An observable absorption shift upon deprotonation requires strong ground- and excited-state communication between protonic functionality and redox chromophore.[16] Such communication is mitigated by a saturated bridge or by canting of the amidinium out of the porphyrin plane.[17−19] In order to circumvent these issues, we now describe the preparation of a homologous set of *meso*- and *β*-alkynylamidinium porphyrin derivatives. As schematically shown in Scheme 1, the protonic functionality is extended away from the macrocycle and, at the same time, electronic communication is preserved between protonic interface and the porphyrin owing to the cylindrical symmetry of an alkyne spacer. The syntheses of the *meso*- and *β*-alkynylamidinium porphyrin derivatives are modular and facile; both have been obtained in just four steps. The benefit of an interposed alkynyl spacer between the amidine and porphyrin is revealed by the strong wavelength dependence of the porphyrin's electronic properties on the amidine/amidinium protonation state. As will be show herein, communication between the porphyrin and amidinium−amidine acid−base functionality may be probed in both the porphyrin ground and excited electronic states.

Experimental Section

Materials. Silica gel 60 (70−230 and 230−400 mesh, Merck) and Merck 60 F254 silica gel (precoated sheets, 0.2 mm thick) were used for column and analytical thin-layer chromatography, respectively. Solvents for synthesis were of reagent grade or better and were dried according to standard methods.[20] Spectroscopic experiments employed CH_3CN (Spectroscopic Grade), which was also dried according to standard methods and stored under vacuum. Mass spectral analyses were performed in the MIT Department of Chemistry Instrumentation Facility (DCIF) or at the University of Illinois Mass Spectrometry Laboratory. 21*H*,23*H*-5,10,15,20-Tetramesityl porphyrin (**1**),[21] 21*H*,23*H*-5,10,15-trimesityl porphyrin (**6**),[22] phenyl cyanate,[23] and chloromethylaluminum amide[24] were prepared using published procedures.

Nickel(II) 2-Bromo-5,10,15,20-tetramesitylporphyrin (2). 21*H*,23*H*-5,10,15,20-Trimesitylporphyrin (300 mg, 0.383 mmol) was dissolved in 350 mL of CH_2Cl_2 and MeOH (9:1 vol/vol) in a 1-L round-bottom flask. The solution was stirred and heated to reflux under air, and 89 mg of NBS (0.50 mmol) was added. After 2 h, the reaction mixture was cooled to room temperature and concentrated in vacuo. The crude material was purified by chromatography on silica using hexanes and CH_2Cl_2 (5:1) as the eluent to provide the freebase 2-bromo-5,10,15,20-tetramesitylporphyrin product. The freebase porphyrin was dissolved in 25 mL of DMF, and a large excess of $Ni(OAc)_2{\cdot}(H_2O)_4$ was added to the solution. The resulting mixture was heated at reflux under a nitrogen atmosphere for 45 min. The resulting dark red solution was then cooled to room temperature, diluted with 200 mL of water, and extracted twice with 50 mL of CH_2Cl_2. The organic extracts were combined, washed several times with water, dried over Na_2SO_4, and then concentrated under reduced pressure. Purification on silica using hexanes and CH_2Cl_2 (3:1) as the eluent delivered 112 mg of the title compound in 32% yield. ^{1}H NMR (300 MHz, $CDCl_3$, 25 °C): δ 8.69 (s, 1H), 8.51 (m, 4H), 8.47 (d, J = 3.3 Hz, 2H), 7.20 (br s, 6H), 7.16 (br s, 2H), 2.56 (s, 9H), 2.55 (s, 3H), 1.82 (s, 12H), 1.77 (s, 6H), 126 (s, 6H). HRESIMS $[M]^+$, *m*/*z*: Calcd for $C_{56}H_{51}BrN_4Ni$, 916.2645. Found, 916.2605.

Nickel(II) 2-(Trimethylsilyl)ethynyl-5,10,15,20-tetramesitylporphyrin (3). Porphyrin **2** (100 mg, 0.109 mmol), $PdCl_2(PPh_3)_2$ (25 mg, 0.035 mmol) and CuI (5 mg, 0.025 mmol) were combined in a 50-mL Schlenk flask. The flask was evacuated and backfilled with nitrogen. Dry DMF and NEt_3 (15 mL, 1:1) were added to the mixture. The solution was heated to 110 °C under nitrogen, and 500 μL of (trimethylsilyl)acetylene was added to the stirred solution. After 40 h, the reaction was cooled to room temperature and the solvent was removed under reduced pressure. The crude material was dissolved in CH_2Cl_2 and washed twice with water (75 mL), and the organic layer was dried over Na_2SO_4. The crude material was purified on silica using hexanes and CH_2Cl_2 (7:1). The title compound was obtained in 72% yield (74 mg). ^{1}H NMR (300 MHz, $CDCl_3$, 25 °C): δ 8.68 (s, 1H), 8.49 (m, 4H), 8.47 (d, J = 3.3 Hz, 2H), 7.19 (br s, 6H), 7.16 (br s, 2H), 2.56 (s, 9H), 2.55 (s, 3H), 1.82 (s, 12H), 1.77 (s, 6H), 1.56 (s, 6H), 0.72 (s, 9H). HRESIMS $[M + H]^+$, *m*/*z*: Calcd for $C_{61}H_{60}N_4NiSi$, 935.4013. Found, 935.4002.

Nickel(II) 2-(Cyano)ethynyl-5,10,15,20-tetramesitylporphyrin (4). The trimethylsilyl-protected porphyrin (**3**) (70 mg, 0.075 mmol) was dissolved in 15 mL of THF and CH_3OH (3:1), and 100 mg (0.1 mol) of K_2CO_3 was added to the stirred solution. The resulting mixture was stirred for 18 h under air. To the mixture, 25 mL of saturated NH_4Cl and 20 mL of CH_2Cl_2 were added. The organic layer was separated, washed twice with 20 mL of saturated NH_4Cl, and dried over Na_2SO_4. The resulting solution was filtered

(11) Cukier, R. I.; Nocera, D. G. *Annu. Rev. Phys. Chem.* **1998**, *49*, 337−369.
(12) Cukier, R. I. *Biochim. Biophys. Acta* **2004**, *1655*, 37−44.
(13) Hammes-Schiffer, S. In *Electron Transfer in Chemistry*; V. Balzani, Ed.; Wiley-VCH: Weinheim, Germany, 2001, Vol. 1.1.5, p 189.
(14) Hammes-Schiffer, S. *Acc. Chem. Res*. **2001**, *34*, 273−281.
(15) Hammes-Schiffer, S.; Iordanova, N. *Biochim. Biophys. Acta* **2004**, *1655*, 29−36.
(16) Rosenthal, J.; Hodgkiss, J. M.; Young, E. R.; Nocera, D. G. *J. Am. Chem. Soc*. **2006**, *128*, 10474−10483.
(17) Yeh, C.-Y.; Miller, S. E.; Carpenter, S. D.; Nocera, D. G. *Inorg. Chem*. **2001**, *40*, 3643−3646.
(18) Deng, Y.; Roberts, J. A.; Peng, S.-M.; Chang, C. K.; Nocera, D. G. *Angew. Chem., Int. Ed.* **1997**, *36*, 2124−2127.
(19) Kirby, J. P.; van Dantzig, N. A.; Chang, C. K.; Nocera, D. G. *Tetrahedron Lett.* **1995**, *36*, 3477−3480.
(20) Armarego, W. L. F.; Perrin, D. D. *Purification of Laboratory Chemicals*, 4th Ed.; Butterworth-Heinmann: Oxford, 1996.
(21) Lindsey, J. S.; Wagner, R. W. *J. Org. Chem*. **1989**, *34*, 828−836.
(22) Shultz, D. A.; Gwaltney, K. P.; Lee, H. *J. Org. Chem*. **1998**, *63*, 4034−4038.
(23) Moss, R. A.; Chu, G.; Sauers, R. R. *J. Am. Chem. Soc*. **2005**, *127*, 2408−2409.
(24) Levin, J. I.; Turos, E.; Weinreb, S. M. *Synth. Commun*. **1982**, *12*, 989−993.

through a short plug of silica and concentrated under reduced pressure. The resultant material was placed in a 50 mL Schlenk tube and dissolved in 10 mL of THF. The purple solution was cooled to −78 °C under a nitrogen atmosphere and 1.75 mL of 1.6 M *n*-BuLi in hexane (2.8 mmol) was added via syringe. The resultant solution was stirred for 90 min, PhOCN (1.0 mL) was added, and the reaction was allowed to warm to room temperature over the course of several hours. To the resulting green solution was added 50 mL of 1 M NaOH, and the biphasic mixture was extracted twice with 100 mL of CH_2Cl_2. The combined organic extracts were washed twice each with brine and water and then dried over Na_2SO_4 and concentrated under reduced pressure. The desired product was purified by chromatography on silica using hexanes and CH_2Cl_2 (4:1) as the eluent to generate 42 mg of the title compound (63% yield). ^{1}H NMR (300 MHz, $CDCl_3$, 25 °C): δ 8.79 (s, 1H), 8.58 (m, 4H), 8.53 (d, J = 3.3 Hz, 2H), 7.24 (br s, 6H), 7.21 (br s, 2H), 2.71 (s, 9H), 2.63 (s, 3H), 1.89 (s, 12H), 1.81 (s, 6H), 1.68 (s, 6H). HRESIMS $[M + H]^+$, *m*/*z*: Calcd for $C_{59}H_{52}N_5Ni$, 888.3571. Found, 889.3536.

Nickel(II) 2-(Amidinium)ethynyl-5,10,15,20-tetramesitylporphyrin chloride (5). To a toluene solution (10 mL) of **4** (25 mg, 0.028 mmol) was added chloromethylaluminum amide (4.0 mL, 1.2 M in toluene) under a nitrogen atmosphere. The reaction solution was heated at 100 °C under nitrogen for 5 days. The resulting solution was then cooled to room temperature, poured slowly onto a slurry of silica gel (15 g) in $CHCl_3$ (30 mL), and stirred under air for 10 min. The slurry was filtered over sintered glass, and the filtercake was washed with CH_2Cl_2/CH_3OH (3:1) until all porphyrin product had been eluted. The filtrate was concentrated under reduced pressure, and the residue purified by column chromatography on silica using CH_2Cl_2 and CH_3OH (10:1) as the eluent to yield 16 mg (59% yield) of the title compound. ^{1}H NMR (300 MHz, $CDCl_3$, 25 °C): δ 10.12 (br s, 4H), 8.72 (s, 1H), 8.57−8.46 (m, 6H), 7.22 (s, 6H), 7.11 (s, 2H), 2.53 (s, 12H), 1.82 (s, 12H), 1.79 (s, 6H), 1.73 (s, 6H). HRESIMS $[M - Cl]^+$, *m*/*z*: Calcd for $C_{59}H_{55}N_6Ni$, 905.3836. Found, 905.3812.

Nickel(II) 5-Bromo-10,15,20-tetramesitylporphyrin (7). *N*-Bromosuccinimide (NBS, 134 mg, 0.752 mmol) was added in one portion to a solution of 21*H*,23*H*-5,10,15-trimesitylporphyrin (500 mg, 0.752 mmol) in chloroform (400 mL), and the reaction was stirred at room temperature under air for 30 min. The solvent was removed, and the residue was purified by column chromatography (silica gel, 1:1 hexanes/dichloromethane) to provide the freebase 5-bromo-10,15,20-trimesitylporphyrin product. The porphyrin was metalated with $Ni(OAc)_2 \cdot (H_2O)_4$ in a manner identical to that described for **2**. The title compound was purified on silica, using hexanes and CH_2Cl_2 (3:1) as the eluent, to deliver 523 mg (87% yield). ^{1}H NMR (300 MHz, $CDCl_3$, 25 °C): δ 9.64 (d, J = 4.5 Hz, 2H), 8.77 (d, J = 4.5 Hz, 2H), 8.57 (s, 4H), 7.23 (s, 6H), 2.61 (s, 6H), 2.68 (s, 3H), 1.84 (s, 6H), 1.89 (s, 12H). HRESIMS $[M + H]^+$, *m*/*z*: Calcd for $C_{47}H_{42}BrN_4Ni$, 799.1946. Found, 799.1938.

Nickel(II) 5-(Trimethylsilyl)ethynyl-10,15,20-tetramesitylporphyrin (8). Starting with 300 mg of **7** (0.375 mmol), the *meso*-alkynyl porphyrin was prepared in a manner identical to that used for β-homolog **3**. The reaction generated 247 mg (81% yield) of the title compound. ^{1}H NMR (300 MHz, $CDCl_3$, 25 °C): δ 9.54 (d, J = 2.6 Hz, 2H), 8.67 (d, J = 2.6 Hz, 2H), 8.53 (br s, 4H), 7.24 (s, 4H), 7.21 (s, 2H), 2.61 (s, 6H) 2.58 (s, 3H), 1.86 (s, 6H), 1.32 (s, 12H), 0.59 (s, 9H). HRESIMS $[M + H]^+$, *m*/*z*: Calcd for $C_{52}H_{50}N_4NiSi$, 817.3231. Found, 817.3217.

Nickel(II) 5-(Cyano)ethynyl-10,15,20-tetramesitylporphyrin (9). Starting with 200 mg of **8**, the *meso*-alkynyl porphyrin was prepared in a manner identical to that used for β-homolog **4**. The reaction generated 119 mg (63% yield) of the title compound. ^{1}H NMR (300 MHz, $CDCl_3$, 25 °C): δ 9.31 (d, J = 2.1 Hz, 2H), 8.69 (d, J = 2.1 Hz, 2H), 8.69 (d, J = 2.3 Hz, 2H), 8.52 (d, J = 2.3 Hz, 2H), 7.23 (s, 4H), 7.20 (s, 2H), 2.59 (s, 6H), 2.56 (s, 3H), 1.82 (s, 6H), 1.57 (s, 12H). HRESIMS $[M + Na]^+$, *m*/*z*: Calcd for $C_{50}H_{42}N_5NiNa$, 792.2608. Found, 792.2614.

Nickel(II) 5-(Amidinium)ethynyl-10,15,20-tetramesitylporphyrin Chloride (10). Starting with 50 mg of **9** (0.065 mmol), the *meso*-alkynyl porphyrin was prepared in a manner identical to that used for β-homolog **5**. The reaction generated 35 mg (67% yield) of the title compound. ^{1}H NMR (300 MHz, $CDCl_3$, 25 °C): δ 10.09 (br s, 4H), 9.52 (br s, 4H), 8.65 (br s, 4H), 8.47 (d, J = 5.8 Hz, 4H), 8.41 (d, J = 5.8 Hz, 4H), 7.17 (s, 2H) 7.09 (s, 4H), 2.55 (s, 3H), 2.46 (s, 6H) 1.79 (s, 6H) 1.72 (s, 12H). HRESIMS $[M - Cl]^+$, *m*/*z*: Calcd for $C_{50}H_{45}N_6Ni$, 787.3054. Found, 787.3032.

Physical Measurements. ^{1}H NMR spectra were recorded at 25 °C in the MIT DCIF on a Varian XL-500, Unity 300 or Mercury 300 spectrometer. All chemical shifts are reported using the standard δ notation in ppm; positive chemical shifts are to a higher frequency from the given reference. Absorption spectra were obtained using a Spectral Instruments 440 Series spectrophotometer.

Absorption spectroscopy on samples of PNi(II) β- and *meso*-alkynylamidinium chloride was performed in a high-vacuum cell comprised of a 1-cm path length clear fused-quartz cuvette (Starna cells) connected to a 10-cm^3 solvent reservoir via a graded seal. High-vacuum Teflon valves were used to seal the cell from the environment and the cuvette from the solvent reservoir.

Steady-state spectroscopic experiments on the Ni(II) porphyrins were performed at concentrations of 9 (*meso*) and 16 (β) μM in acetonitrile to give an optical density of ∼0.85 (*meso*) and ∼0.48 (β) AU at the Soret absorption band and ∼0.07 (*meso*) and ∼0.03 (β) AU at the Q_{10} absorption band. Sample preparation was performed under high vacuum. An aliquot of Ni(II) porphyrin (2.7×10^{-8} (*meso*) and 4.6×10^{-8} (β) mol) was added to the cuvette, and the cell was evacuated under high vacuum (10^{-5} Torr) to remove the transferring solvent. Three milliliters of dry acetonitrile were vacuum-transferred to the solvent reservoir where it was subject to three freeze−pump−thaw cycles. The cell was sealed to the environment and removed from the high-vacuum manifold. A titration with 4-dimethylaminopyridine (DMAP) was performed to monitor the spectral shifts associated with deprotonation of the amidinium functionality. Prior to each DMAP addition, acetonitrile was vacuum-transferred to the cuvette with a dry ice/acetone bath and sealed from the solvent reservoir and environment. This procedure ensured that the solvent volume remained constant throughout the course of the experiment. A stock solution of DMAP was added to the open solvent reservoir, while preserving the vacuum in the cuvette, and the transferring solvent was removed with a high-vacuum manifold (10^{-5} Torr). The solvent reservoir was then sealed from the environment and opened to the cuvette compartment to introduce each new DMAP addition.

A Benesi−Hildebrand plot was developed for the spectral shift of the Soret band ($1/\Delta A_{Soret}$ vs 1/[DMAP]) of PNi(II) upon its titration with DMAP. The Soret band of *meso*-substituted Ni(II) porphyrin is observed at 422 nm with a measured extinction coefficient of 94 000 M^{-1} cm^{-1}, while the Soret band of the β-substituted PNi(II) is observed at 432 nm with an extinction coefficient of 32 500 M^{-1} cm^{-1}. Titration with DMAP yields strong isosbestic points for both the *meso*- and β-substituted PNi(II) systems. Because an isosbestic point occurs near the Soret peak of the amidinium, as opposed to that of the amidine porphyrin, the absorption changes associated with the Soret band of the latter (ΔA_{Soret}) were used in the Benesi−Hildebrand analysis. A 2-nm

Scheme 2

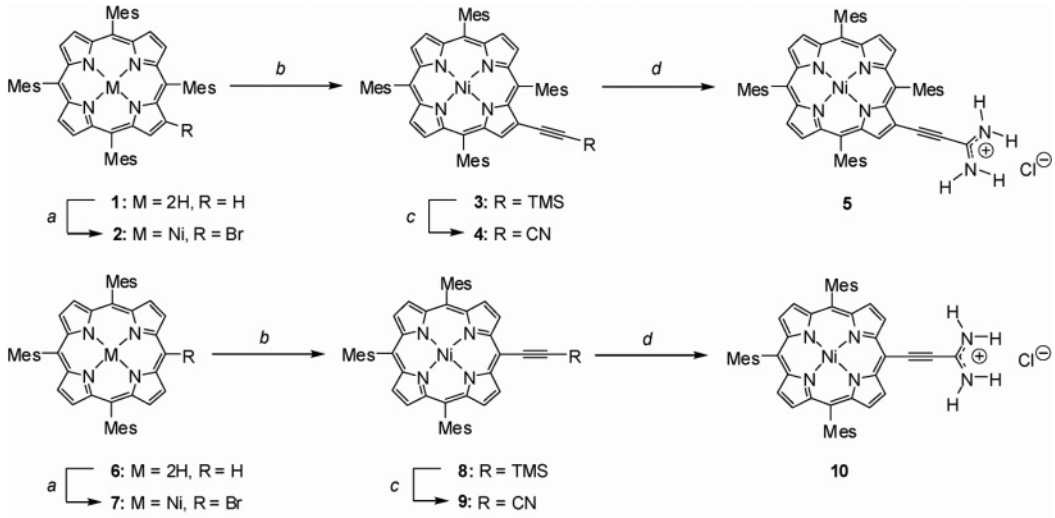

a) 1. NBS, CH_2Cl_2, CH_3OH; 2. Ni(OAc)$_2$, DMF; b) (Trimethylsilyl)acetylene, CuI, $PdCl_2(PPh_3)_2$, NEt_3, DMF; c) 1. K_2CO_3, THF, CH_3OH; 2. PhLi, THF; 3. PhOCN; d) $AlCl(CH_3)(NH_2)$, toluene.

blue-shift is observed in the *meso*-substituted porphyrin spectra to a final Soret peak position at 420 nm, while the β-substituted porphyrin Soret undergoes a 3-nm red-shift to 435 nm. An acidity constant, K_a, for *meso*- and β-substituted Ni(II)P is obtained from the ratio of the *y* intercept and slope of linearly fit data.[25]

Computations. Density functional theory (DFT) and time-dependent density functional theory (TDDFT) calculations were performed using the Amsterdam Density Functional (ADF2006.01, TDDFT; ADF2004.01, DFT) program[26−28] on a home-built Linux cluster comprising 60 Intel processors organized in groups of 12 running in parallel. The generalized gradient approximation was used as implemented in ADF by the Becke exchange functional,[29] and the PW91c correlation functional.[30] Convergence criteria tolerance for DFT was altered from default and set as follows. Energy, 1×10^{-4} Hartrees; gradients, 1×10^{-3} Hartrees; coordinates, 1×10^{-3} Å; bond angles, 0.5°. Relativistic corrections were included using the scalar zero-order regular approximation (ZORA).[31,32] A basis set of triple-ζ Slater-type functions augmented by a polarization set (TZP) was used for Zn and N atoms and double-ζ with polarization (DZP) was used for C and H. Relativistic frozen core approximation was used to treat shells up to 2p for Zn and 1s for C and N as core shells. Orbitals were visualized using the Molekel v.4.2 Linux-mesa software.[33,34]

TDDFT was utilized for calculations on the protonated (amidinium) and deprotonated (amidine) functionalities of both Ni(II) porphyrins. Calculations were performed in which the plane of the amidinium functionality was rotated with respect to the porphyrin plane. The final coordinates of an initial DFT geometry optimization were utilized as the input coordinates. The dihedral angle ($\theta_{dihedral}$), defined by the N−C_{amH+} bond of the amidinium and the C_β−C_α or C_{meso}−C_α and on the porphyrin ring, was rotated by intervals of 10° and restrained. Default convergence criteria were used for rotated calculations.

Results and Discussion

Alkynyl amidinium functionalities were fused to either the β (**5**) or *meso* (**10**) positions of the mesityl porphyrin macrocycle following the synthetic protocol outlined in Scheme 2. **1** was the starting material of choice for the synthesis of the β-alkynyl amidinium derivative, owing to the superior solubilizing properties of the mesityl groups on the porphyrin periphery. Bromination of **1** using NBS gives **2**,[35] which may be Sonagashira coupled to trimethylsilylacetylene to cleanly generate alkynyl porphyrin **3**. Following deprotection of the alkynyl group using tetrabutylammonium fluoride, lithiation and reaction with phenyl cyanate provides β-alkynyl cyano porphyrin **4**. The nitrile is transformed to the corresponding amidinium **5** using an excess of Weinreb's amide transfer reagent[36] under harsh conditions (100 °C, 5 days). *meso*-Alkynyl amidinium porphyrin **10** is prepared along similar lines to the β-homolog, using **6** as the starting material. The synthesis of **5** and **10** in just four steps each represents a dramatic improvement over previously prepared amidinium porphyrin derivatives, which are prepared via arduous 26- and 12-step synthetic routes.[16,37]

Electronic coupling between the amidinium functionality and porphyrin macrocycle is signified by the pH dependence of the electronic absorption spectra of both the β- and *meso*-

(25) Connors, K. A. In *Binding Constants: A Measurement of Molecular Complex Stability*; Wiley: New York, 1987.
(26) *ADF2004.01, SCM, Theoretical Chemistry*; Vrije Universiteit: Amsterdam, The Netherlands, http://www.scm.com.
(27) te Velde, G.; Bickelhaupt, F. M.; van Gisbergen, S. J. A.; Fonseca Guerra, C.; Baerends, E. J.; Snijders, J. G.; Ziegler, T. *J. Comput. Chem.* **2001**, *22*, 931−967.
(28) Fonseca Guerra, C.; Snijders, J. G.; te Velde, G.; Baerends, E. J. *Theor. Chem. Acc.* **1998**, *99*, 391- 403.
(29) Becke, A. D. *Phys. Rev. A* **1988**, *38*, 3098−3100.
(30) Perdew, J. P.; Chevary, J. A.; Vosko, S. H.; Jackson, K. A.; Pederson, M. R.; Singh, D. J.; Fiolhais, C. *Phys. Rev. B* **1992**, *46*, 6671−6687.
(31) Van Lenthe, E.; Baerends, E. J.; Snijders, J. G. *J. Chem Phys.* **1993**, *99*, 4597−4610.
(32) Van Lenthe, E.; Ehlers, A.; Baerends, E. J. *J. Chem. Phys.* **1999**, *110*, 8943−8953.
(33) Flükiger, P.; Lüthi, H. P.; Portmann, S.; Weber, J. *Molekel v.4.2/3*; Swiss Center for Scientific Computing: Manno, Switzerland, 2000−2002.
(34) Portmann, S.; Lüthi, H. P. *Chimia* **2000**, *54*, 766−769.
(35) Zhou, X.; Tse, M. N.; Wan, T. S. M.; Chan, K. S. *J. Org. Chem.* **1996**, *61*, 3590−3593.
(36) Levin, J. I.; Turos, E.; Weinreb, S. M. *Synth. Commun.* **1982**, *12*, 989−993.
(37) Deng, Y.; Roberts, J. A.; Peng, S. M.; Chang, C. K.; Nocera, D. G. *Angew. Chem., Int. Ed. Engl.* **1997**, *36*, 2124−2127.

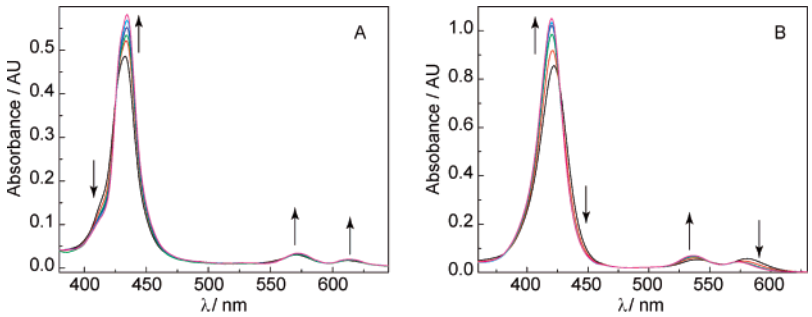

Figure 1. Spectral changes associated with deprotonation of (a) amidinium porphyrin **5** and (b) amidinium porphyrin **10** in CH_3CN.

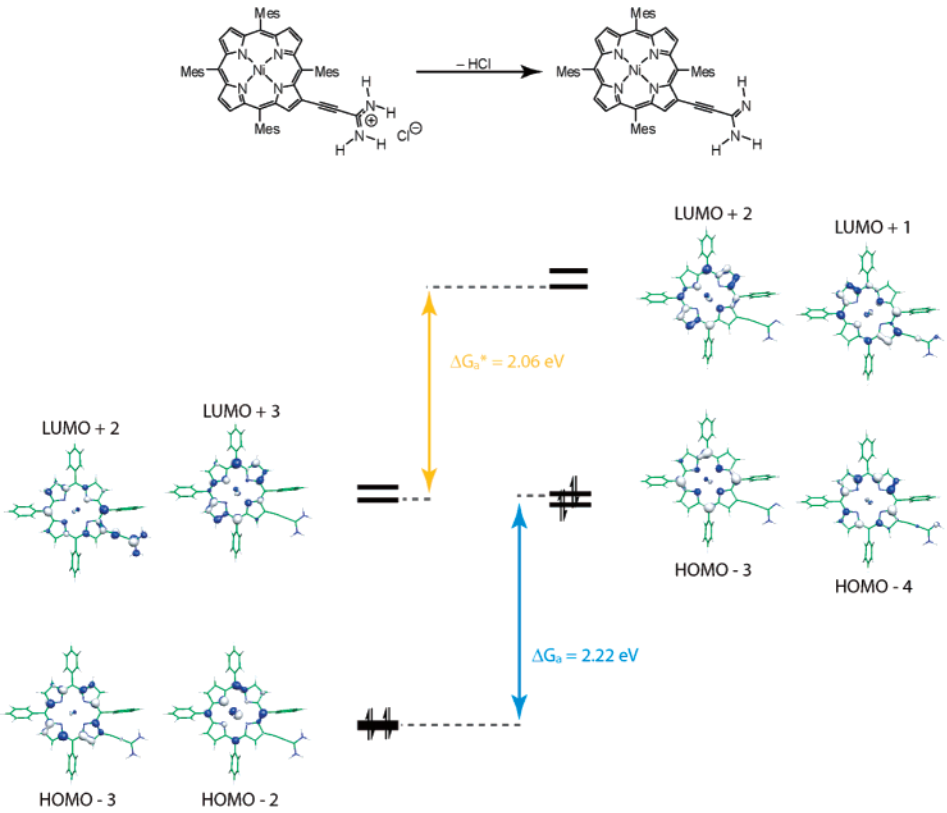

Figure 2. Frontier molecular orbitals that contribute to the observed electronic transitions for both the amidinium and amidine forms of amidinium porphyrin **5**, which is a photoacid. The energies shown are calculated for the visualized orbitals by TDDFT.

alkynyl amidinium porphyrins. Figure 1A shows an experimentally observable perturbation of the UV−vis absorbance profile of **5** upon deprotonation of the amidinium group. A bathochromic shift is observed for the Soret band from 432 to 435 nm upon deprotonation of the amidinium. Well-anchored isosbestic points are maintained at 425, 564, and 602 nm between the spectra of the protonated (amidinium) and deprotonated (amidine) forms of the proton interface. The red-shift in the Soret band is accompanied by similar spectral shifts in the *Q*-band region. The absorption spectrum of the *meso*-alkynyl amidinium **10** also displays alteration upon deprotonation of the amidinium functionality. However, as shown in Figure 1B, a hypsochromic shift is observed upon conversion of amidinium to amidine. The maximum of the Soret band shifts from 422 to 420 nm while maintaining well-anchored isosbestic points at 428, 550, and 568 nm. Similar modulation of the absorption profile is observed in the *Q*-band region of **10** upon deprotonation.

The electronic coupling responsible for spectral shifts associated with the protonation state of the amidine is reflected by geometry-optimized TDDFT and DFT calculations for the porphyrin molecular orbitals of **5** and **10**. Two factors dominate the coupling: the electronic structure of the frontier molecular orbitals of the porphyrin ring at the *meso*- and *β*-positions and the twist angle of the acid−base group with regard to the porphyrin ring. The results of these TDDFT and DFT calculations offer qualitative insight toward the experimental behavior of **5** and **10**, as shown in Figures 2−4. Although these computations do not incorporate a dielectric solvent model, they provide a qualitative picture of the orbital and energetic perturbations associated with amidinium deprotonation of porphyrins **5** and **10**. Such comparisons have previously been shown to be useful.[16]

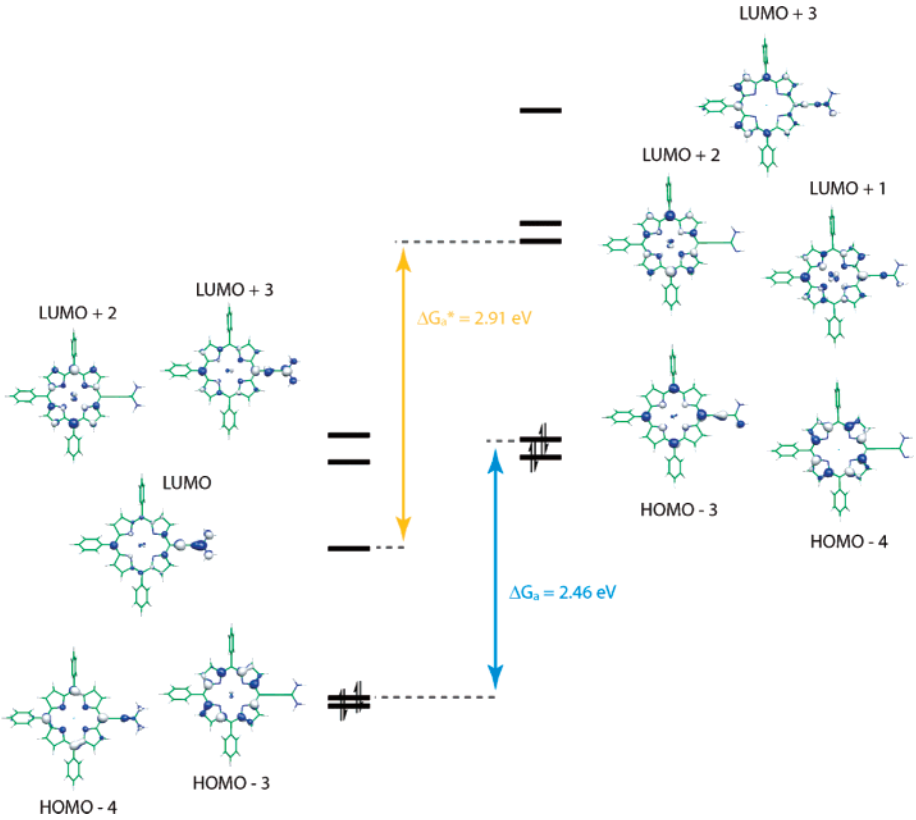

Figure 3. Frontier molecular orbitals that contribute to the observed electronic transitions for both the amidinium and amidine forms of amidinium porphyrin **10**, which is a photobase. The energies shown are calculated for the visualized orbitals by TDDFT.

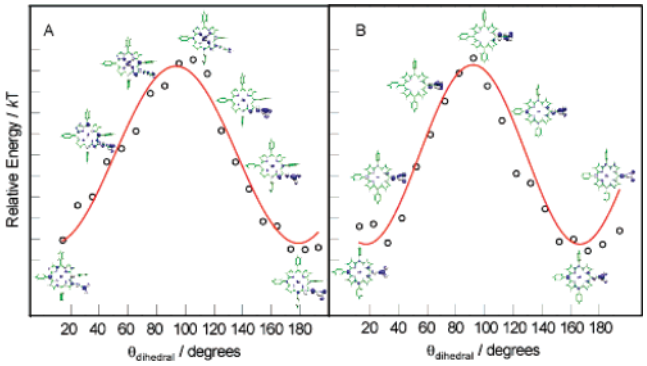

Figure 4. Relative potential energies of (A) β-alkynylamidinium porphyrin (**5**) and (B) *meso*-alkynylamidinium porphyrin (**10**) are shown as the dihedral angle defining the plane of the porphyrin relative to the amidinium is rotated and restrained. The LUMO+3 of **5** and the LUMO of **10**, the two lowest lying unoccupied orbitals with significant porphyrin π-orbital and substituent density are shown at θ (relative to θ_i) = 0°, 30°, 60°, 90°, 120°, 165°, 180°.

DFT calculations may reasonably predict electronic transition wavelengths for optical absorptions in porphyrins with β and *meso* substituents.[38−43] The calculated porphyrin frontier orbitals of **5** and **10** are shown in Figures 2 and 3, respectively, for both the alkynylamidinium acid (left) and the corresponding conjugate alkynylamidine base (right). Molecular orbitals lacking significant porphyrin π-orbital character are omitted for clarity, as they are not responsible for the porphyrin transitions observed in the absorption profiles of Figure 1. Considering the electronic distribution about the porphyrin ring, it has been shown that HOMOs of a_{2u} and a_{1u} symmetries result in maximal orbital overlap with alkyne groups in *meso*- and β-positions, respectively.[44−46] In the systems described here, these orbitals are the parents of the HOMO-3 and HOMO-4 orbitals shown for **5** in Figure 2 and HOMO-4 and HOMO-3 orbitals for **10** shown in Figure 3. These orbitals, which are the highest occupied porphyrin-based MOs, provide the linchpin for electronic coupling of the alkynyl group to the porphyrin ring. The energy gap is affected not only by the sensitivity of the aforementioned porphyrin-based HOMO levels on protonation state but dependent on the LUMOs as well. The LUMO+2 and LUMO+1 of protonated and deprotonated **5** (Figure 2) and the LUMO, LUMO+3 and the LUMO+1, LUMO+3 of the protonated and deprotonated **10** (Figure 3) show orbital density on both the porphyrin macrocycle and

(38) Walsh, P. J.; Gordon, K. C.; Officer, D. L.; Campbell, W. M. *Theochem.* **2006**, *759*, 17−24.
(39) Liao, M-S.; Scheiner, S. *Chem. Phys. Lett.* **2003**, *367*, 199−206.
(40) Cramariuc, O.; Hukka, T. I.; Rantala, T. T. *Chem. Phys.* **2004**, *305*, 13−26.
(41) Nguyen, K. A.; Day, P. N.; Pachter, R. *J. Phys. Chem. A* **2000**, *104*, 4748−4754.
(42) van Gisberg, S. J. A.; Rosa, A.; Ricciarde, G.; Baerends, E. J. *J. Chem. Phys.* **1999**, *111*, 2499−2506.
(43) Sundholm, D. *Phys. Chem. Chem. Phys* **2000**, *2*, 2275−2281.
(44) Strachan, J.−P.; Gentemann, S.; Seth, J.; Kalsbeck, W. A.; Lindsey, J. S.; Holten, D.; Bocian, D. F. *J. Am. Chem. Soc.* **1997**, *119*, 11191−11201.
(45) Yang, S. I.; Seth. J.; Balasubramanian, T.; Kim, D.; Lindsey, J. S.; Holten, D.; Bocian, D. F. *J. Am. Chem. Soc.* **1999**, *121*, 4008−4018.
(46) Holten, D.; Bocian, D. F.; Lindsey, J. S. *Acc. Chem. Res.* **2003**, *35*, 57−69.

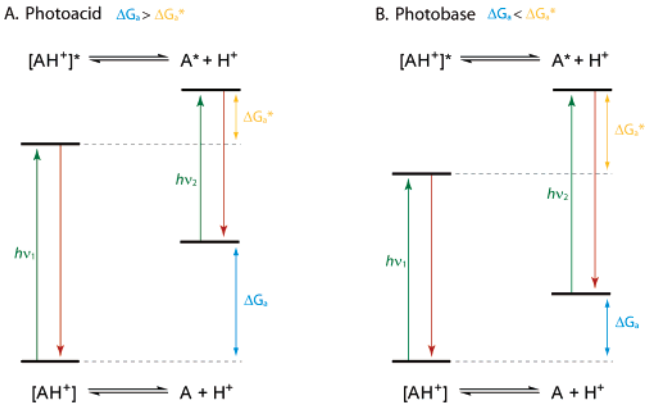

Figure 5. Generalized Jablonski diagrams of (a) molecular species that behave as photoacids and (b) molecular species that behave as photobases.

the alkynylamidinium functionality. This electronic redistribution is responsible for the spectral sensitivity of the porphyrin to the amidinium protonation state.

The calculations shown in Figure 4 predict a $\theta_{dihedral} = 14°$ for β-alkynylamidinium porphyrin **5** and a $\theta_{dihedral} = 12°$ for *meso*-alkynylamidinium porphyrin **10**. These relatively small cant angles contrast sharply with the roughly 75° cant angle calculated for previously studied porphyrin−amidinium compounds in which the amidinium was directly linked to the porphyrin.[17,19] The steric clashing between the amidinium and hydrogens of the porphyrin ring that plagues a direct linkage is avoided by poising the amidinium at the end of the ethynyl linker of **5** and **10**. The electronic structure of the alkynyl spacer is cylindrically symmetric and hence the electronic communication between the amidinium and porphyrin macrocycle should be perturbed minimally with rotation. Systematic variation of $\theta_{dihedral}$ to span angles between 0° and 180° confirms the intuition that conjugation persists upon amidinium rotation. Molecular orbitals and relative orbital energies for rotational calculations on **5** and **10** are presented in Figures S1 and S2 in the Supporting Information.

A sense for the barrier of rotation can be gleaned from the calculated potential energy of the system upon rotation of amidinium as shown in Figure 4.[47,48] The potential energy change relative to the geometry optimized calculation in terms of kT varies as

$$\Delta U(\theta) = U(\theta) - U(\theta_i) \qquad (1)$$

where $U(\theta) = A \sin[\omega(\theta - \theta_c)]$ and θ_i is the initial cant angle for the system, $\theta_i = 14.4$ for β-alkynylamidinium and $\theta_i = 12.7$ for *meso*-alkynylamidinium. A is the amplitude of the sine curve, ω is related to the period of oscillation, and θ_c is the offset angle. Fitted values for β-alkynylamidinium are $A = 4.21\ kT$, $\omega = 2.11$, and $\theta_c = 50.7°$ and *meso*-alkynylamidinium are $A = 4.27\ kT$, $\omega = 2.42$, and $\theta_c = 54.7°$ Two times the fitted amplitude ($2A$) represents the barrier height for rotation of the alkynylamidinium functionality: 8.42 kT (4.99 kcal/mol) for β-alkynylamidinium and 8.54 kT (5.05 kcal/mol) for *meso*-alkynylamidinium.

The spectral signatures accompanying deprotonation of the amidinium functionalities of alkynyl porphyrins **5** and **10** provide observables that can be used to determine the pK_a of the amidinium in the porphyrin in its ground and excited electronic states. Titration of **5** in CH_3CN with the base DMAP produces the spectral series shown in Figure 1A. A Benesi−Hildebrand plot of the spectral shifts (see Figure S3 in the Supporting Information) yields a deprotonation constant (K_a'), from which the pK_a of **5** may be determined according to the relation

$$pK_a(PNi(II)) = pK_a(DMAP) - \log(K_a') \qquad (2)$$

The pK_a of DMAP in CH_3CN is 12.33,[49] yielding a pK_a = 7.03 ± 0.10 for the ground state of β-alkynyl amidinium porphyrin **5**. In its excited state ([AH$^+$]*), **5** is predicted to be a stronger acid than in its ground state since the absorption spectrum of the conjugate base displays a bathochromic shift relative to that of the conjugate acid ($h\nu_1 > h\nu_2$).[50−53] This follows from the simplified Jablonski diagram shown in Figure 5. The thermodynamic relationship between the ground and excited states for a proton-containing species (AH$^+$) and its conjugate base (A) predict that its excited state ([AH$^+$]*) is a stronger acid than the ground state when a bathochromic shift accompanies acid deprotonation ($h\nu_1 > h\nu_2$). Put another way, the free energy change associated with deprotonation of the molecule in the excited state (ΔG_a*) is less than that for deprotonation in the ground state (ΔG_a). The excited-state acidity constant, pK_a*, is formalized by the Förster equation,[53,54]

$$pK_a^* = \Delta G_a^*/2.3RT = pK_a - (h\nu_1 - h\nu_2)/2.3RT \qquad (3)$$

For eq 3, $h\nu_1$ and $h\nu_2$ represent the energies of the 0−0 electronic transitions for the conjugate acid and base, respectively. Analysis of the electronic absorption spectra associated with deprotonation of **5** leads yields a pK_a* = 6.89 ± 0.10 in CH_3CN at 23 °C. These results demonstrate that the acidity of **5** is greater in its excited-state as compared to its ground state (pK_a = 7.03 ± 0.10).

Using eq 2 and the K_a' determined from the Benesi−Hildebrand plot obtained for **10** (Figure S4 in the Supporting Information), the ground-state pK_a for *meso*-alkynyl amidinium porphyrin **10** is calculated to be 7.74 ± 0.10, which is similar to that of **5**. However, in contrast to **5**, **10** is photobasic. In its excited state ([AH$^+$]*), **10** is more basic

(47) Okuno, Y.; Kamikado, T.; Yokohama, S.; Mashiko, S. *Theochem.* **2002**, *594*, 55−60.
(48) Crossely, M. J.; Field, L. D.; Forster, A. J.; Harding, M. M.; Sternhell, Sever. *J. Am. Chem. Soc.* **1987**, *109*, 341−348.
(49) Izutsu, K. *Acid-Base Dissociation Constants in Dipolar Aprotic Solvents*; Blackwell Scientific: Cambridge, MA, 1990.
(50) Ireland, J. F.; Wyatt, P. A. H. *Adv. Phys. Org. Chem.* **1976**, *12*, 131−160.
(51) Shizuka, H. *Acc. Chem. Res.* **1985**, *18*, 141−147.
(52) Arnaut, L. G.; Formosinho, S. J. *J. Photochem. Photobiol. A* **1993**, *75*, 1−20.
(53) Tolbert, L. M.; Solntsev, K. M. *Acc. Chem. Res.* **2002**, *35*, 19−27 and references therein.
(54) Weller, A. *Z. Elektrochem.* **1952**, *56*, 662−668.

than in its ground state, as indicated by the hypsochromic shift of the conjugate base relative to that of the conjugate acid ($h\nu_1 < h\nu_2$) since ΔG_a^* is greater than ΔG_a (Figure 5B).[50−52] Following eq 3, the excited-state pK_a of **10** is determined to be 8.37 ± 0.10.

The disparate behavior of the acidity properties of **5** and **10** in their ground and excited states is reflected in the energetics arising from the β- and *meso*-alkynylamidinium substitution pattern. The energy differences calculated by TDDFT between HOMOs of the protonated and deprotonated forms of **5** in Figure 2 is $\Delta G_a = 2.22$ eV, whereas the LUMOs energy difference is $\Delta G_a^* = 2.06$ eV, respectively. Given that $\Delta G_a > \Delta G_a^*$, porphyrin **5** is predicted to be a photoacid in accordance with the experimentally observed bathochromic shift observed upon deprotonation of **5**. The same TDDFT calculations were carried out for the *meso*-alkynylamidinium porphyrin (**10**), the results of which are shown in Figure 3. Unlike the β-amidinium derivative, porphyrin **10** shows the opposite trend for the relative values of ΔG_a and ΔG_a^*. A third low-lying LUMO orbital with significant alkynylamidinium and porphyrin π-orbital density is evident in the protonated *meso*-alkynylamidinium molecular orbitals resulting in an increased ΔG_a^* value. Values of $\Delta G_a = 2.46$ eV and $\Delta G_a^* = 2.91$ eV are found for porphyrin **10**. As a result, $\Delta G_a < \Delta G_a^*$ and porphyrin **10** is predicted to be a photobase, in agreement with the observed absorption shifts.

In summary, amidiniums substituted at the β and *meso* positions of porphyrins maintain electronic communication with the macrocycle via ethynyl spacers. A facile and modular synthesis of the alkynyl amidinium homologs permits the arduous synthesis accompanying direct linkage of amidiniums directly to the porphyrin to be avoided. Both congeners display similar ground-state acidity constants but exhibit opposite trends in terms of relative acidity upon photoexcitation. β-Alkynylamidinium porphyrin (**5**) is photoacidic, whereas the *meso*-alkynylamidinium porphyrin (**10**) is photobasic. These disparate properties invite the possibility of probing the role of excited-state acidity in promoting PCET reactivity through hydrogen bonding interfaces.

Acknowledgment. J.R. thanks the Fannie and John Hertz Foundation for a predoctoral fellowship. This work was supported by the National Institutes of Health GM GM47274.

Supporting Information Available: Molecular orbitals and UV−vis data. This material is available free of charge via the Internet at http://pubs.acs.org.

IC700838S